NEURAL REGENERATION RESEARCH
www.nrronline.org

Research Article

Tropism-shifted AAV-PHP.eB-mediated *bFGF* gene therapy promotes varied neurorestoration after ischemic stroke in mice

Rubing Shi[1], Jing Ye[1], Ze Liu[1], Cheng Wang[1], Shengju Wu[1], Hui Shen[1], Qian Suo[1], Wanlu Li[1], Xiaosong He[2], Zhijun Zhang[1], Yaohui Tang[1], Guo-Yuan Yang[1, *], Yongting Wang[1, *]

https://doi.org/10.4103/NRR.NRR-D-23-01802

Date of submission: November 2, 2023

Date of decision: January 31, 2024

Date of acceptance: March 26, 2024

Date of web publication: July 10, 2024

From the Contents

Graphical Abstract

Altered AAV-PHP.eB tropism promotes distinct functional recovery in a mouse model of ischemic stroke subjected to bFGF gene therapy

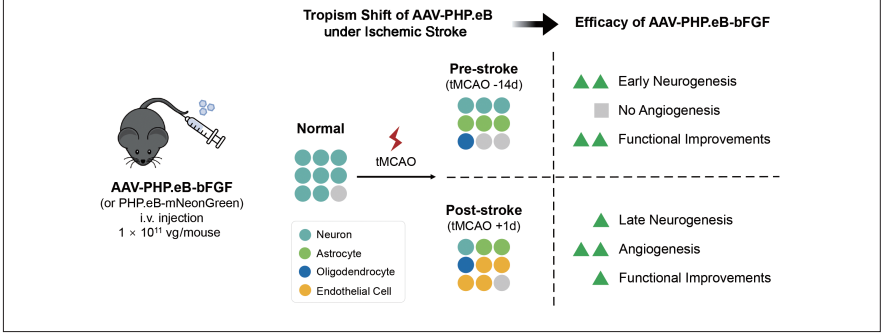

Abstract

AAV-PHP.eB is an artificial adeno-associated virus (AAV) that crosses the blood–brain barrier and targets neurons more efficiently than other AAVs when administered systematically. While AAV-PHP.eB has been used in various disease models, its cellular tropism in cerebrovascular diseases remains unclear. In the present study, we aimed to elucidate the tropism of AAV-PHP.eB for different cell types in the brain in a mouse model of ischemic stroke and evaluate its effectiveness in mediating basic fibroblast growth factor (*bFGF*) gene therapy. Mice were injected intravenously with AAV-PHP.eB either 14 days prior to (pre-stroke) or 1 day following (post-stroke) transient middle cerebral artery occlusion. Notably, we observed a shift in tropism from neurons to endothelial cells with post-stroke administration of AAV-PHP.eB-mNeonGreen (mNG). This endothelial cell tropism correlated strongly with expression of the endothelial membrane receptor lymphocyte antigen 6 family member A (Ly6A). Furthermore, AAV-PHP.eB-mediated overexpression of bFGF markedly improved neurobehavioral outcomes and promoted long-term neurogenesis and angiogenesis post–ischemic stroke. Our findings underscore the significance of considering potential tropism shifts when utilizing AAV-PHP.eB-mediated gene therapy in neurological diseases and suggest a promising new strategy for *bFGF* gene therapy in stroke treatment.

Key Words: AAV-PHP.eB; angiogenesis; basic fibroblast growth factor; gene therapy; ischemic stroke; Ly6A; neurogenesis; neurological function; transient middle cerebral artery occlusion; tropism

Introduction

Adeno-associated viruses (AAVs) have been used extensively as vehicles to mediate gene transfer to the central nervous system (CNS). AAV-PHP.eB is a newly-developed AAV that penetrates the blood–brain barrier (BBB) more efficiently than other AAV vectors, enabling gene delivery to the CNS through intravenous injection at a relatively low viral load of 1×10^{11} vector genomes (vg)/mouse (Chan et al., 2017). Due to its neurotropism and brain-wide expression span, AAV-PHP.eB is a useful tool for conditional knock-in/-out mouse strain construction (Xiao et al., 2021; Zhou et al., 2022), calcium imaging (Grødem et al., 2023), brain-wide gene expression mapping (Matsumoto et al., 2019), and retrograde tracing of neurons (Han et al., 2022). Multiple studies have explored AAV-PHP.eB tropism, as well as variations on its effects when used via different administration routes, in different mouse strains, and with different cell-specific promoters (Xie et al., 2021; Jang et al., 2022; Liu et al., 2022). In addition, AAV-PHP.eB has been shown to be a promising vector for CNS gene therapies in preclinical studies using rodent models of conditions such as hearing loss, Alzheimer's disease, and spinal cord injury (Sun et al., 2020; Zheng et al., 2022; Aljović et al., 2023). However, the cellular tropism of AAV-PHP.eB in cerebrovascular diseases remains incompletely understood.

Ischemic stroke is one of the leading causes of mortality and morbidity worldwide (GBD 2019 Stroke Collaborators, 2021). Currently, the most effective treatments are tissue plasminogen activator thrombolysis and endovascular thrombectomy. However, the narrow therapeutic time window and the limited number of eligible patients mean that there is an urgent need to develop novel therapies for patients who cannot receive these treatments. Gene therapy is a potential treatment option for ischemic stroke, owing to recent developments in gene delivery systems and promising results from clinical studies of other diseases. These advances have made it possible to

[1]Med-X Research Institute and School of Biomedical Engineering, Shanghai Jiao Tong University, Shanghai, China; [2]Department of Emergency, the Second Affiliated Hospital, Department of Human Anatomy, School of Basic Science, Guangzhou Medical University, Guangzhou, Guangdong Province, China
***Correspondence to:** Yongting Wang, PhD, yongting.wang@gmail.com; Guo-Yuan Yang, MD, PhD, gyyang@sjtu.edu.cn.
https://orcid.org/0000-0003-3105-9307 (Guo-Yuan Yang); https://orcid.org/0000-0002-5841-6557 (Yongting Wang)

Funding: *This study was supported by the National Natural Science Foundation of China, Nos. 81870921 (to YW), 81974179 (to ZZ), 82271320 (to ZZ), 82071284 (to YT); National Key R&D Program of China, No. 2022YFA1603600 (to ZZ), 2019YFA0112000 (to YT); Scientific Research and Innovation Program of Shanghai Education Commission, No. 2019-01-07-00-02-E00064 (to GYY); Scientific and Technological Innovation Act Program of Shanghai Science and Technology Commission, No. 20JC1411900 (to GYY).*
How to cite this article: *Shi R, Ye J, Liu Z, Wang C, Wu S, Shen H, Suo Q, Li W, He X, Zhang Z, Tang Y, Yang GY, Wang Y (2026) Tropism-shifted AAV-PHP.eB-mediated bFGF gene therapy promotes varied neurorestoration after ischemic stroke in mice. Neural Regen Res 21(2):704-714.*

revisit therapeutic candidates that did not meet primary endpoints in previous trials by using AAV-PHP.eB to stabilize the expression of the target genes and the encoded proteins.

Basic fibroblast growth factor (bFGF) plays multiple roles in both physiological and pathological processes in the CNS. In preclinical stroke studies, bFGF has been shown to attenuate apoptosis, improve cell survival, and promote angiogenesis and neurogenesis (Chen et al., 1994; Wang et al., 2008; Jiang et al., 2017; Sun et al., 2018; Li et al., 2023; Duan et al., 2024; Wu et al., 2024). However, in a clinical trial of treatment for acute stroke based on a previous preclinical study (Fisher et al., 1995), bFGF showed no significant advantage over placebo in terms of its ability to confer neuroprotection and decrease infarct volume, mainly because it induced dose-dependent hypotension and increased mortality (Bogousslavsky et al., 2002). These effects may be because recombinant bFGF was administered intravenously and has a short half-life *in vivo* (Lazarous et al., 1997) owing to its low molecular weight (~22 kDa). Despite these limitations of bFGF when administered systemically during the acute phase of disease in clinical trials, increasing evidence from preclinical studies has shown that bFGF promotes neurogenesis (Wang et al., 2008), axonal sprouting (Kawamata et al., 1997), angiogenesis (Ito et al., 2022), and behavioral recovery. Therefore, recent research has focused on developing bFGF therapy options that exhibit longer, more stable expression (Sheng et al., 2018; Wang et al., 2022b) and induce fewer side effects (such as increased immune responses).

The aims of this study were to identify the cellular tropism of AAV-PHP.eB in an adult C57BL/6J mouse model of ischemic stroke and to test the efficacy of AAV-PHP.eB-mediated *bFGF* gene therapy on angiogenesis, neurogenesis, and neurological recovery.

Methods

AAV-PHP.eB production and purification

AAV (serotype PHP.eB) was produced by OBiO Technology Corp., Ltd. (Shanghai, China). Briefly, AAV-293 cells were triple-transfected with pAAV-CMV-mNeonGreen-3FLAG/pAAV-CMV-FGF2-P2A-mNeonGreen-3FLAG, pHelper, and the cargo plasmid pAAV-PHP.eB RC. Seventy-two hours after transfection, the cells were lysed and centrifuged along with the medium, and the supernatants containing the virus were collected. Then, the virus was purified by ultracentrifugation in an iodixanol gradient and ultrafiltration. Finally, the viral titer was determined by quantitative polymerase chain reaction (qPCR).

Animals

All animal experiments were performed following Animal Research: Reporting of *In Vivo* Experiments (ARRIVE) guidelines (Percie du Sert et al., 2020) and were approved by the Institutional Animal Care and Use Committee of Shanghai Jiao Tong University, Shanghai, China (animal ethics protocol number 2022008; approval date: August 1, 2022). Adult male C56BL6/J mice (total n = 129, 8–10 weeks of age, 22–24 g in weight) were purchased from Beijing Vital River Laboratory Animal Technology Co., Ltd. (Beijing, China; animal license No. SCXK (Hu) 2017-0011) and housed in a specific pathogen-free animal room under a 12-hour light/dark cycle at 20–26°C with 40%–60% humidity.

For the tropism experiments, 66 mice were randomly divided into the healthy, sham, and transient middle cerebral artery occlusion (tMCAO) groups. The tMCAO animals were then divided into a pre-stroke group and a post-stroke group. For the *bFGF* gene therapy experiments, 63 mice were divided into the sham, pre-control, pre-bFGF, post-control, and post-bFGF groups. Details of the group assignments are shown in **Tables 1** and **2**.

AAV-PHP.eB-mNeonGreen (mNG) or AAV-PHP.eB-bFGF was administered intravenously via the tail vein at a dose of 1×10^{11} vg/mouse in 100 µL sterilized normal saline (Meilunbio, Shanghai, China) 14 days before or 1 day after tMCAO. 5-Bromo-2′-deoxyuridine (BrdU, Beyotime, Shanghai, China) and 2′-deoxy-5-ethynyluridine (EdU, Beyotime) were administered intraperitoneally at a dose of 50 mg/kg/day diluted in phosphate-buffered saline (PBS, Meilunbio).

Table 1 | **Total animal number in tropism study**

			Tropism			BrdU	Ly6A: qPCR+FC			iv-IF	
Group	**Treatment/assay**		**7 d**	**14 d**	**28 d**	**14 d**	**1 d**	**3 d**	**7 d**	**14 d**	**Total**
Healthy	Healthy + AAV-mNG		3	3	3					→3	9
Pre-stroke	tMCAO + AAV-mNG	–14 d iv (2)		3	3	3					9
Post-stroke		+1 d iv (2)		3	3	3				→3	9
		+3 d iv (1)								3	3
		+7 d iv (1)								3	3
Sham	Sham						6				6
tMCAO	tMCAO (3)						6	6	6		18
	Total		3	9	9	6	12	6	6	6	57(9)

"→" means the number has been counted in previous mentioned sections. Numbers in the parentheses refer to the animals excluded from further assays based on the tMCAO criteria. AAV: Adeno-associated virus; BrdU: 5-bromo-2′-deoxyuridine; FC: flow cytometry; IF: immunofluorescence; iv: intravenous injection; Ly6A: lymphocyte antigen 6 family member A; mNG: mNeonGreen; qPCR: quantitative polymerase chain reaction; tMCAO: transient middle cerebral artery occlusion.

Table 2 | **Total animal number in gene therapy study**

			Behavioral test		Ki67	EdU	qPCR&ELISA	
Group	**Treatment/assay**		**mNSS**	**Grid Walking & Hanging Wire**	**14 d**	**28 d**	**28 d**	**Total**
Sham	Sham						3	3
Pre-control	tMCAO (8)	–14 d iv +AAV-mNG	10	→6	3	→4	→3	13
Pre-bFGF		–14 d iv +AAV-bFGF	10	→6	3	→4	→3	13
Post-control		+1 d iv +AAV-mNG	10	→6	3	→4	→3	13
Post-bFGF		+1 d iv +AAV-bFGF	10	→6	3	→4	→3	13
	Total		40		12		3	55(8)

"→" means the number has been counted in previous mentioned sections. Numbers in the parentheses refer to the animals excluded from further assays based on the tMCAO criteria. AAV: Adeno-associated virus; EdU: 2′-deoxy-5-ethynyluridine; ELISA: enzyme-linked immunosorbent assay; iv: intravenous injection; mNG: mNeonGreen; mNSS: modified neurological severity score; qPCR: quantitative polymerase chain reaction; tMCAO: transient middle cerebral artery occlusion.

tMCAO mouse model establishment

The tMCAO model was established as described (Lemmerman et al., 2022). In brief, animals were anesthetized with 1.5% isoflurane (RWD Life Science, Shenzhen, China) in oxygen/nitrous oxide (30%/70%). A 6-0 suture (Covidien, Dublin, Ireland) with one end coated with 1.5 mm-long silicone (Kulzer, South Bend, IN, USA) was inserted from the external carotid artery into the internal carotid artery and advanced to the origin of the left middle cerebral artery to occlude it. After 90 minutes the suture was withdrawn to allow reperfusion. Cerebral blood flow was monitored with a laser Doppler flowmeter (Moor Instrument, Devon, UK) at +2 mm M-L from bregma to confirm successful occlusion (10% of baseline) and reperfusion (more than 70% of baseline). Animals that failed to meet the criteria for successful tMCAO were excluded from further assays. Animals in the sham group underwent the same procedure without occlusion of the middle cerebral artery.

Neurobehavioral assessments

All neurobehavioral assessments were performed by an investigator blinded to the experimental group assignments.

The modified neurological severity score (mNSS) was used to assess overall neurological outcomes, as previously described (Jiang et al., 2017). Scores ranged from 0 to 12, with a higher score indicating more severe damage to motor and vestibular function (Schaar et al., 2010).

The grid walking test was performed as previously described (Shi et al., 2021). Each animal was placed in the middle of an elevated grid-walking apparatus for 3 minutes, and footsteps were recorded by video for post-test analysis. Any step that fell into a hole in the grid was considered a foot fault. The foot-fault index was calculated using the following formula: (contralateral faults – ipsilateral faults)/total steps × 100%.

The hanging wire test was performed to evaluate grip strength, balance, and endurance (Balkaya et al., 2013). Briefly, each animal was suspended vertically by its fore-paws from a wire running parallel to the ground. The number of times each mouse fell from the wire within a 180-second time period and the time it took to fall were recorded. Mice that did not fall within this time period were assigned a score of 10, and 1 point was deducted for each fall. The holding impulse was calculated by multiplying animal weight (grams) by the longest time that elapsed between falls (seconds).

Cell proliferation assay

BrdU and EdU easily enter proliferating cells and stably bind to newly synthesized DNA (Salic and Mitchison, 2008), and are thus commonly used to assess cell proliferation. Here, we used BrdU to detect proliferation of mNG-positive astrocytes. BrdU dissolved in PBS to a concentration of 10 mg/mL was administered via intraperitoneal injection at a dose of 50 mg/kg/day for 7 consecutive days after tMCAO and AAV-PHP.eB-mNG administration. Astrocyte proliferation in the brain was then assessed via immunostaining, as described below.

EdU was used to detect proliferating cells that were positive for doublecortin (DCX, a marker of immature neurons) or cluster of differentiation 31 (CD31, an endothelial cell marker) to evaluate the effect of AAV-PHP.eB-bFGF on neurogenesis and angiogenesis after tMCAO. EdU was administered via intraperitoneal injection at a dose of 50 mg/kg/day (10 mg/mL in PBS) from day 14 to day 28 after tMCAO to all four tMCAO groups in the bFGF gene therapy experiments. Proliferation was assessed using a BeyoClick™ EdU Cell Proliferation Kit with Alexa Fluor 594 (Beyotime) according to the manufacturer's instruction.

Immunofluorescence staining

The animals were euthanized with pentobarbital sodium (100 mg/kg in PBS, Glpbio, Montclair, CA, USA), followed by transcardial perfusion with PBS and 4% paraformaldehyde. The brains were collected, fixed in 4% paraformaldehyde (Sinopharm, Beijing, China) for 4 hours and dehydrated in 30% sucrose (Sinopharm) at 4°C for 2 days. Then, the samples were placed in precooled isopentane for 20 seconds and stored at –80°C. The area of the brain where the corpus callosum connects to where the hippocampus first appears (anterior–posterior axis: +1.18 mm to –0.82 mm from bregma) was then sliced into 30-µm-thick coronal sections at –20°C (Paxinos and Franklin, 2001; Shi et al., 2021).

Immunostaining was performed as previously described (Jiang et al., 2017). Brain sections were placed in 0.3% Triton X-100 and blocked with 5% bovine serum albumin, then incubated with primary antibodies at 4°C overnight. For BrdU staining, sections were placed in 2 M HCl for 45 minutes, and rinsed in a sodium tetraborate solution (pH = 8.5). The next day, the sections were incubated with secondary antibodies at 37°C for 1 hour.

The primary antibodies used are as follows: rabbit-anti-neuronal nuclei (NeuN, 1:200, Millipore, Burlington, MA, USA, Cat #abn78, RRID: AB_10807945), rabbit-anti-S100 calcium binding protein B (S100β, 1:200, Proteintech, Rosemont, IL, USA, Cat# 15146-1-AP, RRID: AB_2254244), rabbit-anti-oligodendrocyte transcription factor 2 (Olig2, 1:200, Abcam, Cambridge, UK, Cat# ab109186, RRID: AB_10861310), goat-anti-CD31 (1:200, R&D Systems, Minneapolis, MN, USA, Cat# af3628, RRID: AB_2161028), rabbit-anti-glial fibrillary acidic protein (GFAP, 1:200, Millipore, Cat# ab5804, RRID: AB_2109645), rat-anti-BrdU (1:200, Abcam, Cat# ab6326, RRID: AB_2313786), rabbit-anti DCX (1:200, Abcam, Cat# ab18723, RRID: AB_732011), rabbit-anti-Ki67 (1:200, Abcam, Cat# ab15580, RRID: AB_443209), and rat-anti-Ki67 (1:200, Invitrogen, Waltham, MA, USA, Cat# 14-5698-80, RRID: AB_10853185). The secondary antibodies included donkey-anti-rabbit IgG, Alexa Fluor 594–conjugated (1:500, Invitrogen, Cat# A21207, RRID:AB_141637), Alexa Fluor 647–conjugated (1:500, Invitrogen, Cat# A31573, RRID: AB_2536183); donkey-anti-goat IgG, Alexa Fluor 555–conjugated (1:500, Invitrogen, Cat# A21432, RRID: AB_141788), Alexa Fluor 647–conjugated (1:500, Invitrogen, Cat# A21447, RRID: AB_2535864), and donkey-anti-rat IgG, Alexa Fluor 594–conjugated (1:500, Invitrogen, Cat# A21209, RRID: AB_2535795).

Quantification was performed for three or four mice from each group based on three coronal sections per mouse that collectively spanned the entire injury region (one rostral, one central, and one caudal, section at 300-µm intervals) and three or four random fields per section taken in the peri-infarct area or subventricular zone (SVZ), using a confocal microscope (Leica, Wetzlar, Germany). Cell and vessel numbers were counted manually, and vessel diameters were measured manually (**Additional Figure 1**), using LAS AF Lite software (Leica). Vessels less than 10 µm in diameter were defined as capillaries.

Cresyl violet staining

Cresyl violet staining was performed as previously described (Jiang et al., 2017). Briefly, 30-µm-thick coronal sections at 300-µm intervals were collected, as described above. The sections were stained with 0.1% cresyl violet solution (Meilunbio) for 3 to 5 minutes and washed with ddH_2O for 10 minutes. The ipsilateral and contralateral areas were measured using Fiji software (Version 2.15.0) (Schindelin et al., 2012). Then, the atrophy volume was calculated using the following formulas: $\Delta S_n = S_{n\_contra} - S_{n\_ipsi.}$ $V = \sum h/3[\Delta S_n + (\Delta S_n \times \Delta S_{n+1})1/2 + \Delta S_{n+1}]$. The brain atrophy ratio (%) = atrophy volume/contralateral volume × 100. "*V*" stands for the atrophy volume; "*S*" stands for the area; "*n*" stands for each slice and "*n*+1" for the next slice; and "*h*" is the interval between slices (300 µm).

Quantitative polymerase chain reaction

The animals were euthanized and transcardially perfused as described earlier. Brain samples from the peri-infarct cortical and striatal tissue were collected by cutting 2-mm-thick coronal slices (anterior-posterior axis: +1.18 mm to –0.82 mm from bregma) from the injured sites. For the sham group, brain tissue samples were collected from the same locations as the tMCAO group and used as the baseline control. Total RNA was extracted with TRIzol reagent (Molecular Research Center, Cincinnati, OH, USA) as previously described (Suo et al., 2023), according to the manufacturer's protocol. The RNA concentrations were measured using a spectrophotometer (Nanodrop 1000, Thermo Fisher Scientific, Waltham, MA, USA). Next, a standardized quantity of RNA (200 ng/sample) from each sample was reverse transcribed into complementary DNA (cDNA) using a cDNA synthesis kit (Yeasen, Shanghai, China). A two-step qPCR process using qPCR SYBR Green Master Mix (Yeasen) was used to quantify gene expression, with glyceraldehyde 3-phosphate dehydrogenase (*GAPDH*) used as the endogenous control. The qPCR primer sequences are listed in **Table 3**.

Table 3 | **qPCR primer sequences**

Gene name	Forward primer sequence (5'–3')	Reverse primer sequence (5'–3')
LY6A	CCT ACC CTG ATG GAG TCT GTG T	CAC GTT GAC CTT AGT ACC CAG G
FGF2	GCG ACC CAC ACG TCA AAC TA	CCG TCC ATC TTC CTT CAT AGC
GAPDH	CAT CAC TGC CAC CCA GAA GAC TG	ATG CCA GTG AGC TTC CCG TTC AG

FGF2: Fibroblast growth factor 2; GAPDH: glyceraldehyde 3-phosphate dehydrogenase; Ly6A: lymphocyte antigen 6 family member A; qPCR: quantitative polymerase chain reaction.

Flow cytometry

Cells were collected from the peri-infarct cortex and striatum using a neuronal tissue dissociation kit (Miltenyi Biotec, Bergisch Gladbach, Germany, Cat# 130-092-628) according to the manufacturer's instruction, then incubated with FITC-Ly6A (Biolegend, San Diego, CA, USA, Cat# 108105, RRID: AB_313342) and PE-CD31 (Invitrogen, Cat# 12-0311-81, RRID: AB_465631) at 4°C for 30 minutes. The cells were then subjected to flow cytometry using a BD FACS-Aria II instrument (BD Biosciences, Franklin Lakes, NJ, USA), and the data were analyzed using FlowJo™ v10.0 Software (BD Biosciences). The median of the Ly6A fluorescence intensity signal in $CD31^+$ cells was used for statistical analysis.

Enzyme-linked immunosorbent assay

Brain samples were collected as described in the qPCR subsection and lysed in radioimmunoprecipitation assay buffer (Millipore) containing a phosphatase inhibitor (Roche, Basel, Switzerland), a protease cocktail inhibitor (Roche), and phenylmethyl sulfonyl fluoride (Sango Biotech, Shanghai, China). The lysates were then analyzed using a mouse bFGF enzyme-linked immunosorbent assay (ELISA) kit (R&D Systems) according to the manufacturer's instructions. All measurements fell within the standard curve generated by the manufacturer-provided recombinant bFGF standard. The data were normalized to the sham group.

Statistical analysis

Sample size was determined based on our data from our pilot study, followed by power and sample size calculations (powerandsamplesize.com). All data were tested for normal distribution (Shapiro-Wilk test) and homogeneity of variances using IBM SPSS Statistics for Windows (Version 26.0, IBM Corp., Armonk, NY, USA). All other statistical tests were performed using GraphPad Prism (version 8.0.2 for windows, GraphPad Software, Boston, MA, USA, www.graphpad.com): normally distributed variables were compared by one-way or two-way analysis of variance, followed by Holm–Sidak correction, and the data are presented as mean ± standard deviation (SD); otherwise, the data were analyzed by Kruskal–Wallis test, with Dunn's correction, and are presented as mean ± confidence interval (CI). $P < 0.05$ were considered statistically significant.

Results

AAV-PHP.eB mostly targets neurons in healthy mice, as expected

To validate previous observations (Chan et al., 2017) on the tropism and transfection efficiency of AAV-PHP.eB, we intravenously injected adult C57BL6/J mice with AAV-PHP.eB-mNG at a dose of 1×10^{11} vg/mouse. Brain samples were collected 1, 2, and 4 weeks after injection (**Figure 1A**), and mNG fluorescence was detected to confirm transfection (**Figure 1B** and **C**). We then performed co-immunostaining for mNG and NeuN, S100β, Olig2, or CD31 to determine whether the transfected cells were neurons, astrocytes, oligodendrocytes, or endothelial cells, respectively (**Figure 1D**). We found most of the mNG signals colocalized with $NeuN^+$ cells, which is consistent with a previous report (Chan et al., 2017). Limited colocalization of mNG with S100β, CD31, and Olig2 was also detected, indicating a small degree of tropism for other cell types (**Figure 1E**). Statistically, there was no significant difference in transfected cell number or cell tropism between 2 and 4 weeks, indicating that AAV-PHP.eB transfection induced stable gene expression 2 weeks after injection.

AAV-PHP.eB shifts its tropism towards astrocytes and endothelial cells after ischemic stroke

Since AAV-PHP.eB was administered systemically, we asked whether cerebrovascular diseases would alter its tropism. To investigate this, we established the tMCAO mouse model to mimic ischemic stroke. Similar to AAV-mediated gene delivery timelines used in preclinical and clinical studies, we injected AAV-PHP.eB-mNG at two different time points: 14 days before (pre-stroke group, similar to preclinical studies testing genetic modulation) or 1 day after (post-stroke group, more relevant for clinical application) ischemic stroke onset (**Figure 2A**). Immunostaining of the peri-infarct area showed that neuronal tropism decreased in both the pre-stroke and post-stroke groups (**Figure 2B–D**) compared with the healthy group at 2 weeks after intravenous injection, with a more significant decline in the post-stroke group (**Figure 2D**).

Altered morphology of mNG^+ cells in the peri-infarct area was also observed (**Figure 2B** and **C**), indicating a shift in cellular tropism towards non-neuronal cells. We found that the number of $mNG^+/S100\beta^+$ cells increased in both stroke groups, with a significant increase at 2 weeks followed by a plateau in the number of double-positive cells (**Figure 2E**), with no significant difference in $mNG^+/Olig2^+$ cells (**Figure 2F**). We also observed a sharp increase in the number of $mNG^+/CD31^+$ cells in the post-stroke group, compared to the healthy group (**Figure 2G**), indicating that viral administration after ischemic stroke induced a shift to endothelial cell tropism. To rule out any variation owing to differences in transfection efficiency, the proportion of double-positive cells in the mNG^+ cells was analyzed, with similar results to the total number of positive cells (**Figure 2H**).

Next, we examined the contralateral hemisphere to determine whether AAV-PHP.eB cellular tropism was only altered within the ipsilateral hemisphere or changed in both hemispheres. Both the cell number and the proportion of cells indicated similar tropism overall in the contralateral brain and the healthy brain, with strong neuronal targeting evident in both the pre-stroke and post-stroke groups (**Additional Figure 2**).

Our data showed the tropism of AAV-PHP.eB towards neurons decreased and increased in astrocytes in both pre-stroke and post-stroke groups, while only post-stroke administration led to a significant endothelial cell tropism.

Altered endothelial cell tropism in the post-stroke group correlated with Ly6A expression after ischemic stroke

Since astrocytes proliferate after ischemic stroke, we next asked whether the apparent increase in astrocytic targeting was due to astrocyte proliferation. To test this, we injected mice that had received AAV-PHP.eB pre-stroke or post-stroke with BrdU (50 mg/kg/day) from day 1 to day 7 after tMCAO and performed immunostaining for GFAP (**Figure 3A** and **B**). Only a few $mNG^+/BrdU^+/GFAP^+$ cells were observed, while a significantly larger number of $mNG^+/GFAP^+$ cells were seen (**Figure 3C**), indicating that the majority of the targeted astrocytes did not arise by proliferation after tMCAO.

We also found that the targeted endothelial cells were mostly located in vessels less than 10 μm in diameter (**Figure 4A** and **B**), indicating preferential targeting to capillary endothelial cells. Given the sharp increase in AAV-PHP.eB targeting to endothelial cells after ischemic stroke and the fact that AAV-PHP.eB transcytosis in endothelial cells relies on its specific receptor Ly6A (Hordeaux et al., 2019; Huang et al., 2019), we asked whether the shift in cellular tropism related to a change in Ly6A expression after ischemic stroke. To test this, we collected samples from the peri-infarct area and examined Ly6A expression at 1, 3, and 7 days after tMCAO (**Figure 4C**). The results showed that Ly6A messenger RNA (mRNA) expression in the peri-infarct region (**Figure 4D**) and Ly6A protein expression in $CD31^+$ endothelial cells (**Figure 4E**) were significantly increased at 1 day after tMCAO compared with the sham group and other time points. These data indicate an increase in Ly6A expression at 1 day post-stroke, which was when we administered AAV-PHP.eB to mice in the post-stroke group.

To determine whether AAV-PHP.eB administered at later timepoints exhibits a similar shift in cellular tropism, we injected the virus at 1, 3, or 7 days after tMCAO and collected samples 14 days after viral administration (**Figure 4F**). We found that the number of $mNG^+/CD31^+$ cells significantly increased when AAV-PHP.eB injected was 1 day after tMCAO, while no significant difference was found when the injection was administered 3 or 7 days after tMCAO, suggesting a correlation between Ly6A expression and endothelial cell targeting (**Figure 4G** and **H**). We also examined the number of $mNG^+/S100\beta^+$ cells after AAV-PHP.eB administration at different timepoints and observed a similar increase in $S100\beta^+$ cell transfection in all three postinjection groups compared with the healthy group, indicating that astrocytic tropism was not impacted by the injection time, nor by differential expression of Ly6A at different time points.

Our data showed the endothelial cell tropism of AAV-PHP.eB in post-stroke group is correlated with Ly6A expression after ischemic stroke.

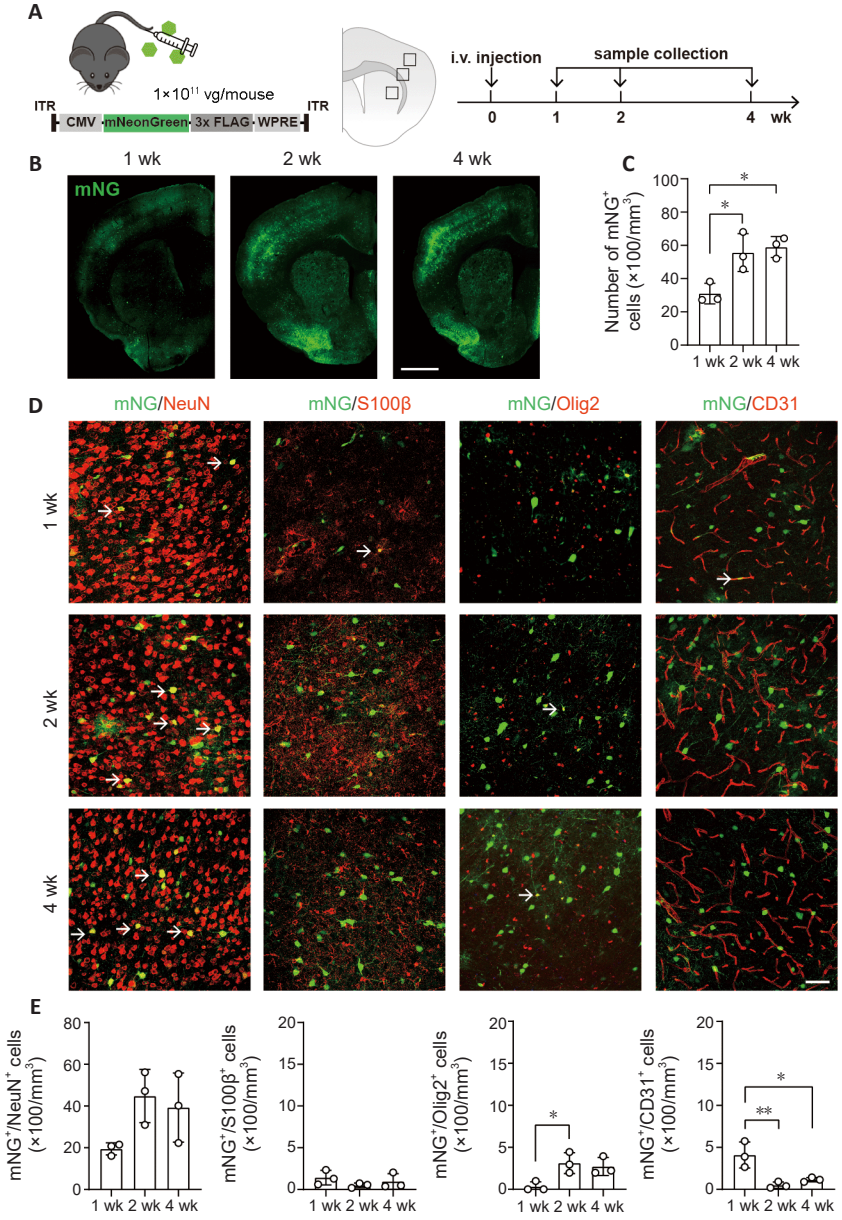

Figure 1 | AAV-PHP.eB mainly targets neurons in healthy mice.

(A) Experimental design and diagram showing where images were taken of brain sections (boxes). (B) Representative coronal sections demonstrating the transfection efficiency of AAV-PHP.eB-mNG in the healthy mouse brain (green: mNG) at 1, 2, and 4 weeks after intravenous injection. Scale bar: 1 mm. (C) Quantification of mNG-positive (mNG$^+$) cells at different time points. The number of mNG$^+$ cells increased 2 weeks after injection and was maintained to 4 weeks. (D) The cellular tropism of AAV-PHP.eB in the brain was analyzed by quantifying colocalization of mNG (green) with cell type markers (red) including NeuN (neurons, Alexa Fluor 594), S100β (astrocytes, Alexa Fluor 594), Olig2 (oligodendrocytes, Alexa Fluor 594), and CD31 (endothelial cells, Alexa Fluor 555). Singal colocalization is indicated with white arrows. Scale bar: 50 μm. (E) Statistical analysis of signal colocalization. The numbers of mNG$^+$/NeuN$^+$ and mNG$^+$/Olig2$^+$ cells increased, while the number of mNG$^+$/CD31$^+$ cells decreased at 2 weeks and was maintained at similar levels 4 weeks after injection. Data are presented as mean ± SD (n = 3 mice/group). *P < 0.05, **P < 0.01 (ordinary one-way analysis of variance followed by Holm–Sidak correction). CD31: Cluster of differentiation 31; mNG: mNeonGreen; NeuN: neuronal nuclei; Olig2: Oligodendrocyte transcription factor 2; S100β: S100 calcium binding protein B.

AAV-PHP.eB-mediated *bFGF* gene therapy promotes functional recovery after ischemic stroke

Based on the altered cellular tropism that we observed, we tested the ability of AAV-PHP.eB-bFGF to promote neurorestoration, rather than neuroprotection, in a mouse model of ischemic stroke by mediating long-term bFGF production in the injured brain. To do this, we injected mice with AAV-PHP.eB-bFGF or AAV-PHP.eB-control 14 days before tMCAO surgery (pre-control and pre-bFGF) or 1 day after tMCAO surgery (post-control and post-bFGF) (**Figure 5A**).

We first confirmed bFGF overexpression in the AAV-PHP.eB-bFGF-treated mice (**Figure 5B** and **C**). Next, we performed cresyl violet staining to evaluate brain atrophy 28 days after tMCAO and found that the brain atrophy ratio was significantly decreased in the pre-bFGF group, while post-stroke AAV-PHP.eB-bFGF administration led to a slight, but not significant, decrease (**Figure 5D** and **E**). Behavioral testing showed that, compared with the AAV-PHP.eB-control-treated groups, AAV-PHP.eB-bFGF-treated mice exhibited continuous improvement in neurological outcomes, with earlier improvements seen in the pre-bFGF group (**Figure 5F** and **G**). Moreover, AAV-PHP.eB-bFGF treatment led to better performance in the hanging wire test 28 days after tMCAO (**Figure 5H**).

Our data showed that AAV-PHP.eB-mediated *bFGF* gene therapy successfully promoted functional recovery after ischemic stroke.

AAV-PHP.eB-mediated *bFGF* gene therapy promotes neurogenesis after ischemic stroke

Next we examined neurogenesis in the ipsilateral SVZ and striatum (**Figure 6A**). The SVZ is enriched in neural stem cells, and after stroke these cells proliferate and migrate towards the peri-infarct area, where they differentiate into functional neurons. This remodeling process ultimately achieves functional repair of the peri-infarct area, including the affected motor cortex (Williamson et al., 2019). The striatum also plays an important role in motor function recovery because it receives synaptic input from the motor cortex to generate certain movements. Motor outcomes are related to the extent of coordinated activity between the cortex and the striatum after ischemic stroke (Guo et al., 2021).

First, we examined neurogenesis by co-staining brain sections collected 2 weeks after tMCAO for Ki67 (cell proliferation marker) and DCX (immature neuron marker) (**Figure 6B**). To explore longer-term neurogenesis, we injected mice with EdU for 2 to 4 weeks after tMCAO, then examined co-localization of EdU and DCX in both the SVZ and the striatum to detect proliferated and migrated neurons (**Figure 6C**). Two weeks after tMCAO, only the pre-bFGF group showed a significant increase in the number of Ki67$^+$/DCX$^+$ cells in SVZ (**Figure 6D**), while both the pre-bFGF and post-bFGF groups exhibited an increase in the number of EdU$^+$/DCX$^+$ cells in the SVZ and striatum (**Figure 6E** and **F**), indicating that AAV-PHP.eB-bFGF strongly promoted neurogenesis.

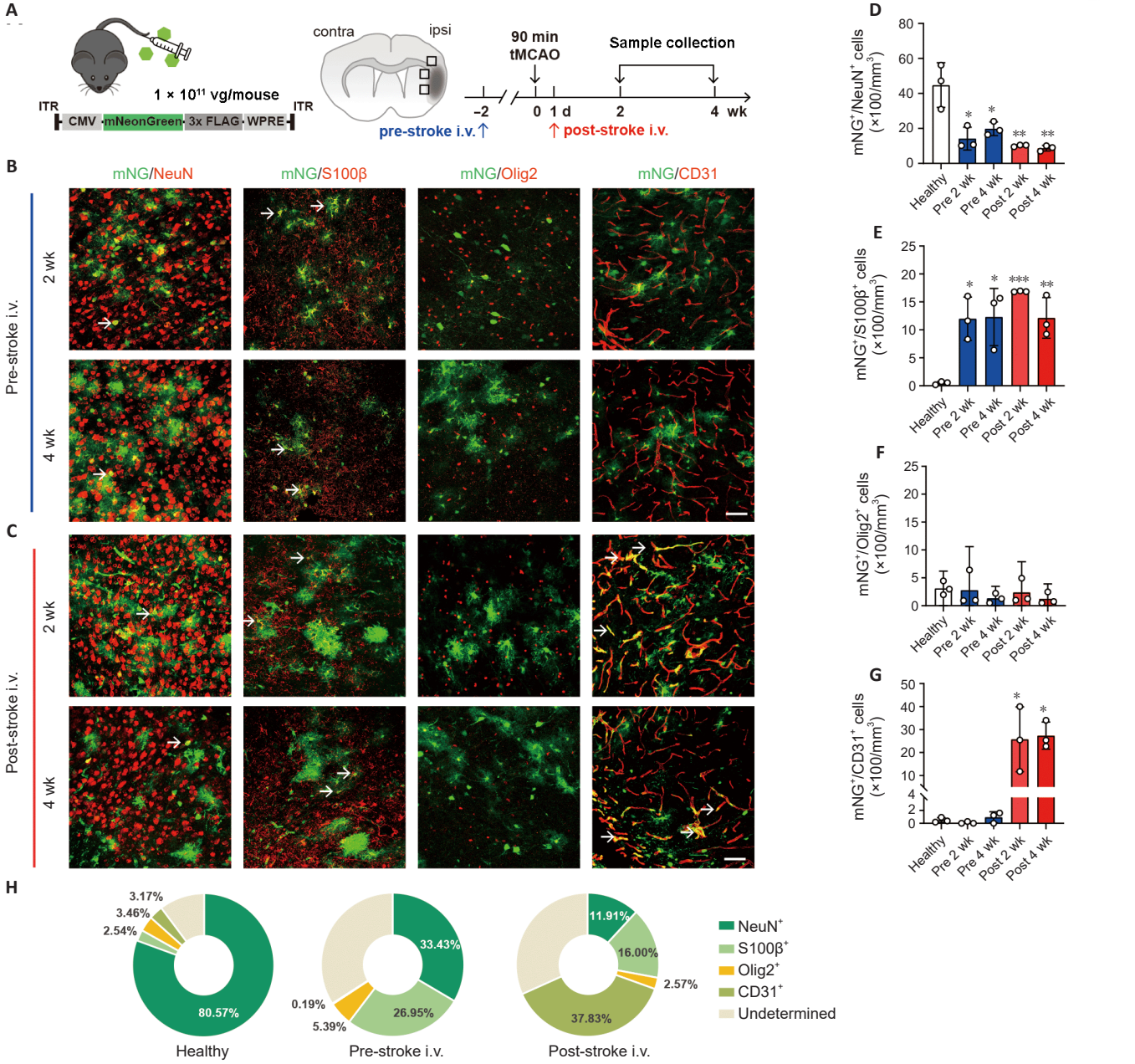

Figure 2 | **The cellular tropism of AAV-PHP.eB in the mouse brain shifted after ischemic stroke.**

(A) Experimental design and diagram showing where images were taken of brain sections (boxes). AAV-PHP.eB-mNG was administered 14 days before tMCAO (pre-stroke group) or 1 day after tMCAO (post-stroke group). (B, C) AAV-PHP.eB-mNG cellular tropism in the ischemic brain was assessed by analyzing colocalization of mNG (green) with other cell type markers (red), including NeuN (neurons, Alexa Fluor 594), S100β (astrocytes, Alexa Fluor 594), Olig2 (oligodendrocytes, Alexa Fluor 594), and CD31 (endothelial cells, Alexa Fluor 555) at 2 and 4 weeks after tMCAO. Signal colocalization is indicated with white arrows. Scale bars: 50 μm. (D–G) Number of mNG^+ cells that colocalized with other cell type markers 2 and 4 weeks after tMCAO, compared with the healthy group 2 weeks after injection. No significant differences were found within the same group at different timepoints. Data are presented as mean ± SD for D, E, and G and mean ± CI for F (n = 3 mice/group). $^*P < 0.05$, $^{**}P < 0.01$, $^{***}P < 0.001$, *vs.* healthy group (ordinary one-way analysis of variance followed by Holm-Sidak correction for D, E, and G and Kruskal–Wallis test followed by Dunn's correction for F). (H) The proportion of mNG^+ cells in the healthy, pre-stroke, and post-stroke groups 4 weeks after intravenous injection. CD31: Cluster of differentiation 31; i.v.: intravenous injection; mNG: mNeonGreen; NeuN: neuronal nuclei; Olig2: oligodendrocyte transcription factor 2; S100β: S100 calcium binding protein B; tMCAO: transient middle cerebral artery occlusion.

AAV-PHP.eB-mediated *bFGF* gene therapy promotes angiogenesis after ischemic stroke

We further examined endothelial cell proliferation in the peri-infarct area (**Figure 7A**) in brain samples from mice injected with EdU from 2 to 4 weeks after tMCAO. The number of $Ki67^+/CD31^+$ cells at 2 weeks (**Figure 7B**) and $EdU^+/CD31^+$ cells at 4 weeks (**Figure 7C**) after tMCAO increased in the post-bFGF group (**Figure 7D** and **E**) but not in the pre-bFGF group, indicating that only post-stroke AAV-PHP.eB-bFGF administration improved angiogenesis after ischemic stroke.

Discussion

In this study, we demonstrated that AAV-PHP.eB exhibits altered cellular tropism after ischemic stroke in mice and that AAV-PHP.eB-mediated *bFGF* gene therapy improves neurological recovery of ischemic stroke in a mouse model.

The tropism of AAV vectors is often influenced by the pathological condition, the choice of promoter, and the administration route. Although cell-specific promoters are ideal for driving cell-specific expression of the target genes, they often leave limited space for the target gene in the vectors (Chai et al., 2023) and sometimes exhibit low levels of expression in other cell types (Wang et al., 2021). Therefore, vectors have been engineered to target specific cell types through the expression of particular peptides on the capsid surface. However, the accurate targeting of these modified capsids is usually tested in healthy animals with a limited range of administration routes. Thus, it is important to carry out tropism studies to ensure that these vectors target the correct cell type under different conditions, and to inform future capsid design by exploring the mechanism of altered tropism.

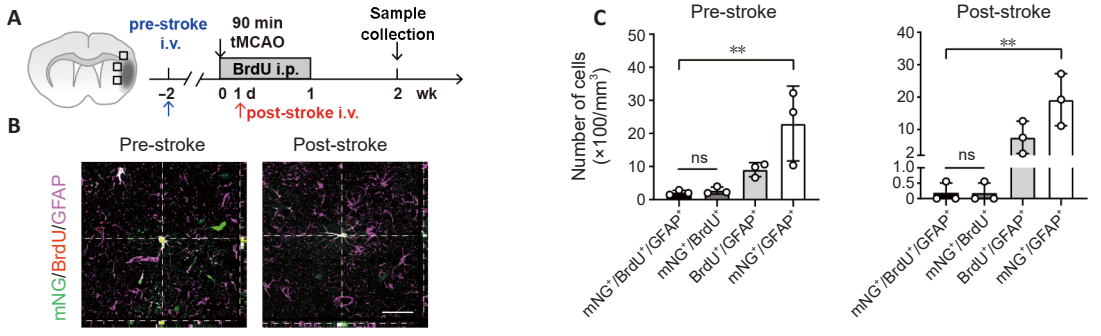

Figure 3 | **AAV-PHP.eB targets astrocytes that do not arise by proliferation after tMCAO.**
(A) Experimental design and diagram showing where images were taken of brain sections (boxes). (B) Representative image of colocalization of mNG (green), BrdU (red, proliferation marker, Alexa Fluor 594), and GFAP (magenta, astrocyte marker, Alexa Fluor 647) in the peri-infarct area 2 weeks after tMCAO in pre-stroke group and post-stroke group. Very few mNG$^+$/BrdU$^+$/GFAP$^+$ cells were observed in both the pre-stroke and post-stroke groups. BrdU/mNG colocalization is shown in yellow, and mNG/GFAP colocalization is shown in white. Scale bar: 25 μm. (C) Statistical analysis of cell numbers. Data are presented as mean ± SD (n = 3 mice/group). $^{**}P < 0.01$ (ordinary one-way analysis of variance followed by Holm-Sidak correction). BrdU: 5-Bromo-2′-deoxyuridine; GFAP: glial fibrillary acidic protein; i.p.: intraperitoneal injection; i.v.: intravenous injection; mNG: mNeonGreen; ns: not significant; tMCAO: transient middle cerebral artery occlusion.

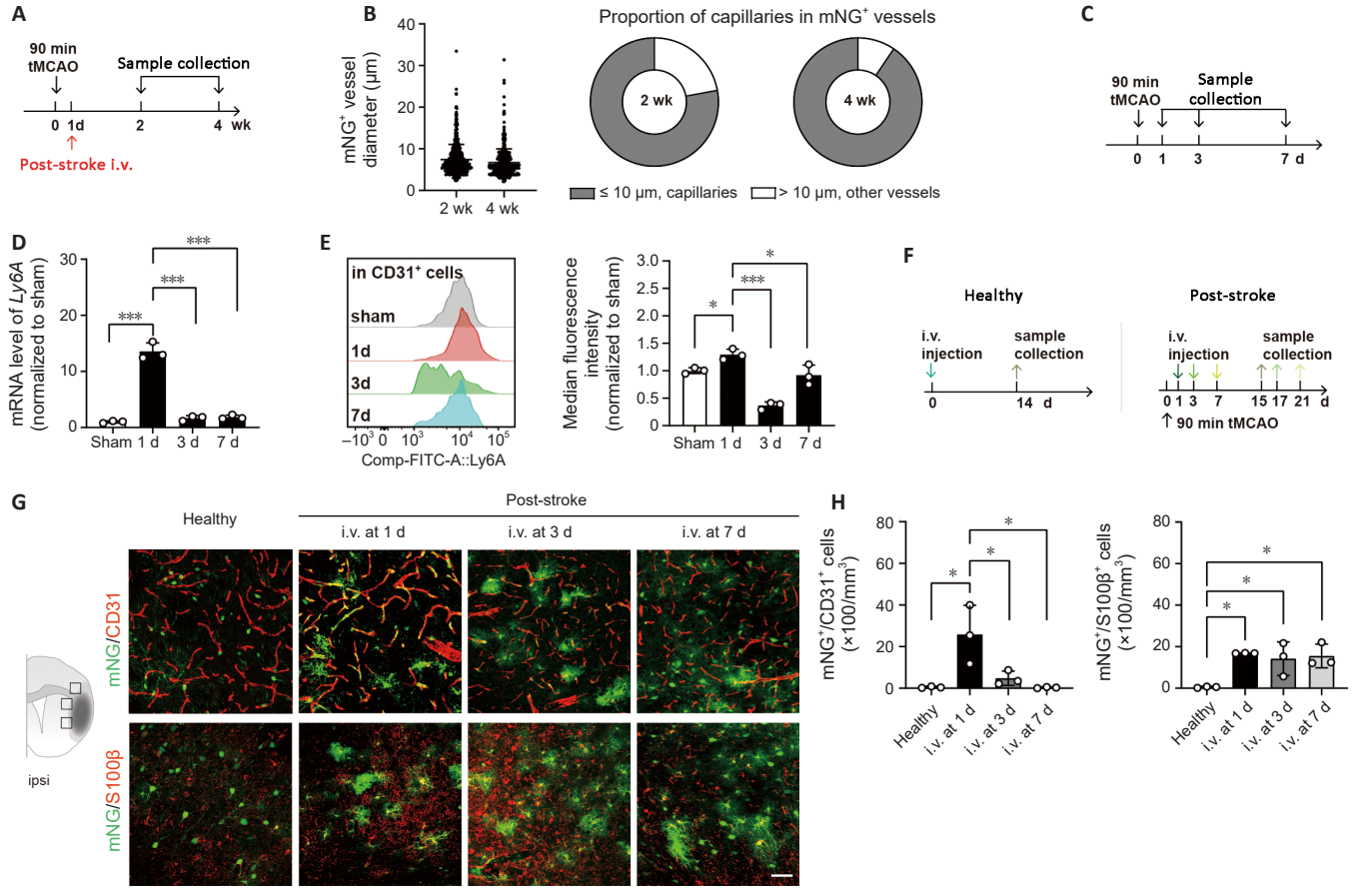

Figure 4 | **Altered AAV-PHP.eB endothelial cell tropism correlates with Ly6A expression after ischemic stroke in mice.**
(A) Experimental design for blood vessel diameter evaluation. (B) Diameter of blood vessels containing mNG$^+$ endothelial cells and proportion of mNG$^+$ capillaries in the post-stroke group 2 and 4 weeks after tMCAO. Vessels less than 10 μm in diameter were defined as capillaries (n = 403 at 2 weeks and 465 at 4 weeks). (C) Experimental design for Ly6A expression assays. (D) *Ly6A* mRNA expression 1, 3, and 7 days after tMCAO. (E) FITC-Ly6A fluorescence intensity in CD31$^+$ endothelial cells 1, 3, and 7 days after tMCAO. (F) Timeline of intravenous AAV-PHP.eB-mNG administration in the healthy group and the post-stroke group. (G) Representative confocal images of mNG (green) colocalization with CD31 (endothelial cell marker, Alexa Fluor 555) and S100β (astrocyte marker, red, Alexa Fluor 594) when AAV-PHP.eB-mNG was administered intravenously 1, 3, and 7 days after tMCAO. The areas where images were taken of brain sections are indicted by boxes. Samples were collected 2 weeks after intravenous administration. Scale bar: 50 μm. (H) Statistical analysis of mNG$^+$/CD31$^+$ and mNG$^+$/S100β$^+$ cell numbers. Data were normalized to data from the sham group, as shown in D and E. Data are presented as mean ± SD (n = 3 mice/group for D, E, and H). $^*P < 0.05$, $^{**}P < 0.01$, $^{***}P < 0.001$ (ordinary one-way analysis of variance followed by Holm-Sidak correction). The number of mNG$^+$/S100β$^+$ increased with poststroke administration at all three timepoints, while the number of mNG$^+$/CD31$^+$ cells only increased with post-stroke injection 1 day after tMCAO. Mice in the healthy group underwent no additional interventions, while sham-operated mice underwent the same tMCAO procedure except suture insertion. CD31: Cluster of differentiation 31; i.v.: intravenous injection; Ly6A: lymphocyte antigen 6 family member A; mNG: mNeonGreen; mRNA: messenger RNA; qPCR: quantitative polymerase chain reaction; S100β: S100 calcium binding protein B; tMCAO: transient middle cerebral artery occlusion.

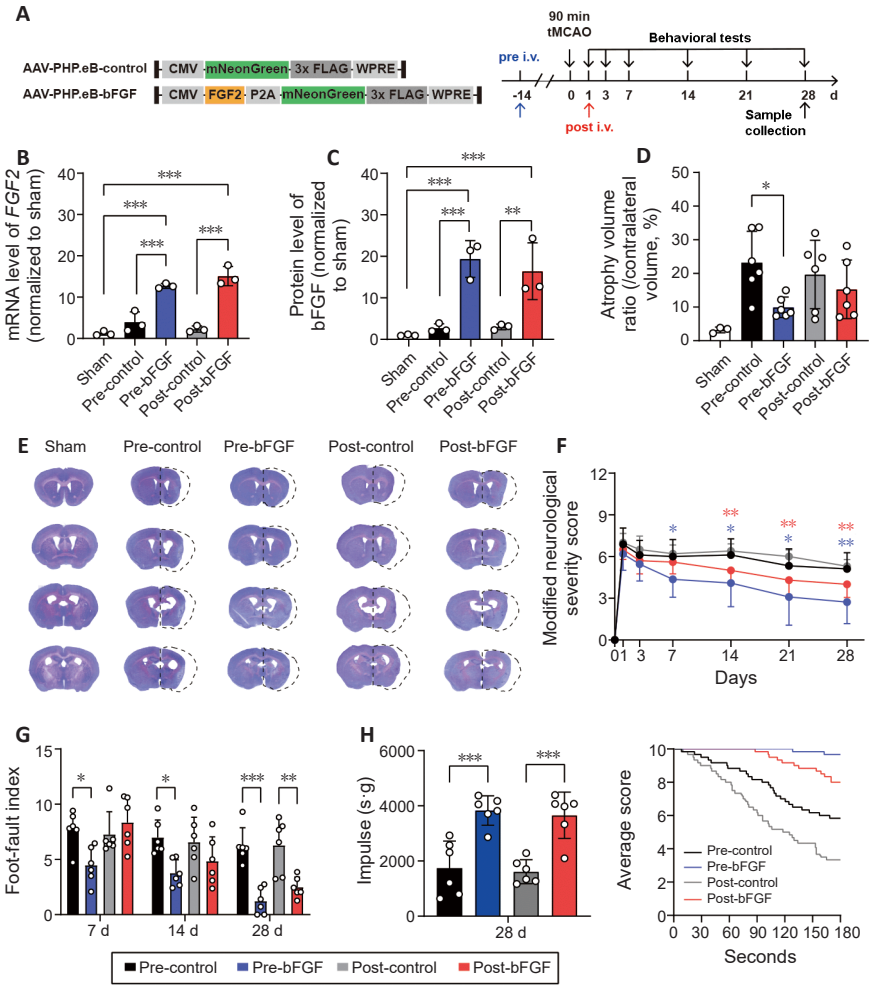

Figure 5 | AAV-PHP.eB-mediated *bFGF* gene therapy promotes functional recovery after ischemic stroke in mice.

(A) Experimental design. Mice were injected with AAV-PHP.eB-control or AAV-PHP.eB-bFGF 14 days before tMCAO (pre-control and pre-bFGF group) or 1 day after tMCAO (post-control and post-bFGF group). (B) *FGF2* mRNA expression in the peri-infarct area of the tMCAO group 4 weeks after tMCAO and in the same anatomical region in the sham group (n = 3 mice/group). (C) bFGF expression 4 weeks after tMCAO (n = 3 mice/group). (D, E) Representative images of cresyl violet-stained brain sections and the ratio of atrophy volume/contralateral hemisphere volume 28 days after tMCAO (n = 6 mice/group). The white area within the dotted line indicates atrophy. Less atrophy was observed in the pre-bFGF group, while no significant difference in atrophy was found in the post-bFGF group, compared with the control groups. (F) mNSS after tMCAO (n = 10 mice/group). (G) Grid walking test results after tMCAO (n = 6 mice/group). (H) Hanging wire test results 28 days after tMCAO (n = 6 mice/group). Data were normalized to data from the sham group, as shown in C and D. Data are presented as mean ± SD. *P < 0.05, **P < 0.01, ***P < 0.001, pre-/post-bFGF group *versus* pre-/post-control group and sham group in B–D, pre-/post-bFGF group *versus* pre-/post-control group in D–F (ordinary one-way analysis of variance followed by Holm-Sidak correction for B–D and H; two-way analysis of variance followed by Holm-Sidak correction for F and G). bFGF: Basic fibroblast growth factor; FGF2: fibroblast growth factor 2; i.v.: intravenous injection; mNSS: modified neurological severity score; mRNA: messenger RNA; tMCAO: transient middle cerebral artery occlusion.

Compared with other AAV variants that rely on direct injection into the brain to bypass the BBB, AAV-PHP.eB penetrates the BBB after administration via intravenous injection, enabling a higher transfection efficiency for CNS neurons at a relatively low dose (Chan et al., 2017; Yuan et al., 2024). Although this virus has been tested in various animal models of disease, its cellular tropism in the context of cerebrovascular disease remains unknown. Since neuronal tropism is mainly driven by the AAV capsid, we chose the nonspecific CMV promoter to drive gene expression in any cell type infected by the virus and compared cellular tropism in healthy mice and mice after ischemic stroke.

We first confirmed the AAV-PHP.eB mediated exogenous gene expression primarily in neurons, with lower expression levels observed in astrocytes and oligodendrocytes and very little expression in endothelial cells, consistent with previous reports (Chan et al., 2017; Mathiesen et al., 2020). Then, we examined the transfected cell types in a mouse model of ischemic stroke. Similar to the timeline of AAV-mediated gene delivery in preclinical and clinical studies, we injected AAV-PHP.eB-mNG 14 days before (pre-stroke group, similar to preclinical studies testing genetic modulation) or 1 day after (post-stroke group, more relevant for clinical application) ischemic stroke onset. We observed a sharp decline in neuronal expression of mNG in both groups, which could have been because of altered cellular tropism or massive neuronal death in the ipsilateral brain triggered by ischemic stroke.

Ischemic stroke increased astrocytic targeting by AAV-PHP.eB in both the pre- and post-stroke groups at both administration timepoints. Though astrocytes proliferate after ischemic stroke (Choudhury and Ding, 2016), our data suggested the increase in mNG^+ astrocytes was not due to astrocytes proliferation. Another possible reason for the observed increase in astrocytic mNG expression could be increased astrocytic endocytosis of cell debris containing mNG after ischemic stroke, which requires further investigation.

In addition to increased astrocytic tropism, we found that, when AAV-PHP.eB-mNG was injected 1 day after stroke, mNG was expressed in many endothelial cells in the peri-infarct area of the brain, most of which were capillary cells. Although we also observed only very low levels of expression of the exogenous gene in endothelial cells in the healthy and pre-stroke groups, the post-stroke group showed a significant increase in exogenous gene expression in endothelial cells compared with the other two groups. Several studies have reported that the Ly6A receptor expressed by brain endothelial cells enables AAV-PHP.eB to penetrate the BBB (Hordeaux et al., 2019; Huang et al., 2019; Batista et al., 2020). In addition, single-cell RNA sequencing showed that Ly6A is primarily expressed by endothelial cells in the CNS (Brown et al., 2021). Therefore, we analyzed Ly6A expression after tMCAO and found that it increased in parallel with increasing AAV-PHP.eB endothelial cell tropism, with both reaching the peak 1 day after tMCAO. A previous *in vitro* study showed that Ly6A overexpression in 293T cells promoted binding and transfection, while blocking Ly6A in brain microvascular endothelial cells led to a significant decrease in transfection (Huang et al., 2019), suggesting a critical role for Ly6A in AAV-PHP.eB endothelial cell targeting. Other possible explanations for the increase in endothelial cell tropism include altered pH in endothelial cells, BBB disruption, endothelial cell dysfunction related to the endosomal system, and differences in transcytosis efficiency (Toth et al., 2018; Andjelkovic et al., 2019; Nian et al., 2020; Kucharz et al., 2021). Future studies should clarify the mechanism of the altered tropism, which will help guide vector design to treat various CNS diseases.

bFGF is mainly expressed in neurons, and its expression in astrocytes increases spontaneously after stroke (Lin et al., 1997). Endogenous bFGF promotes cell survival and proliferation after ischemic stroke (Calvani et al., 2006). Although a clinical study showed that administration of exogenous bFGF increased mortality and the incidence of side effects such as hypotension (Bogousslavsky et al., 2002), bFGF is still being tested in preclinical studies for stroke therapy

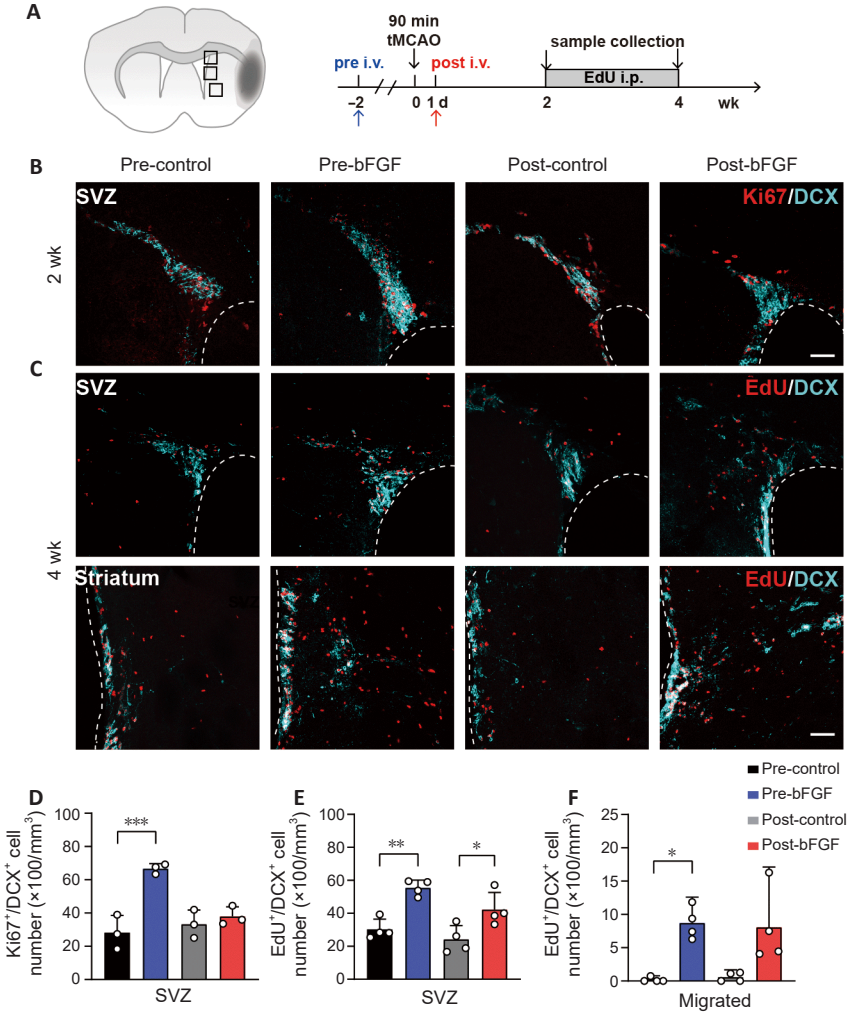

Figure 6 | AAV-PHP.eB-mediated *bFGF* gene therapy promotes neurogenesis after ischemic stroke in mice.
(A) Experimental design and diagram showing where images were taken of brain sections (boxes). Mice were injected with AAV-PHP.eB-control or AAV-PHP.eB-bFGF 14 days before tMCAO (pre-control and pre-bFGF group) or 1 day after tMCAO (post-control and post-bFGF group). (B) Representative confocal images of colocalization of Ki67 (proliferation marker, Alexa Fluor 594, red) and DCX (immature neuron marker, Alexa Fluor 647, cyan) in the ipsilateral SVZ 2 weeks after tMCAO (n = 3 mice/group). Scale bar: 50 μm. The number of $Ki67^+/DCX^+$ cells increased in the pre-bFGF group, while no significant difference was found in the post-bFGF group, compared with the control groups. (C) Representative images of colocalization of EdU (proliferation marker, Alexa Fluor 594, red) and DCX (Alexa Fluor 647, cyan) in the ipsilateral SVZ and peri-infarct striatum 4 weeks after tMCAO (n = 4 mice/group). Scale bar: 50 μm. The number of EdU^+/DCX^+ cells increased in both the pre-bFGF group and the post-bFGF group compared with the control groups. (D–F) Statistical analysis of the numbers of cells exhibiting signal colocalization. Data are presented as mean ± SD for D and E and mean ± CI for F. $^*P < 0.05$, $^{**}P < 0.01$, $^{***}P < 0.001$ (ordinary one-way analysis of variance followed by Holm-Sidak correction for D and E, Kruskal-Wallis test followed by Dunn's correction for F). bFGF: Basic fibroblast growth factor; DCX: doublecortin; EdU: 2′-deoxy-5-ethynyluridine; i.p.: intraperitoneal injection; i.v.: intravenous injection; SVZ: subventricular zone; tMCAO: transient middle cerebral artery occlusion.

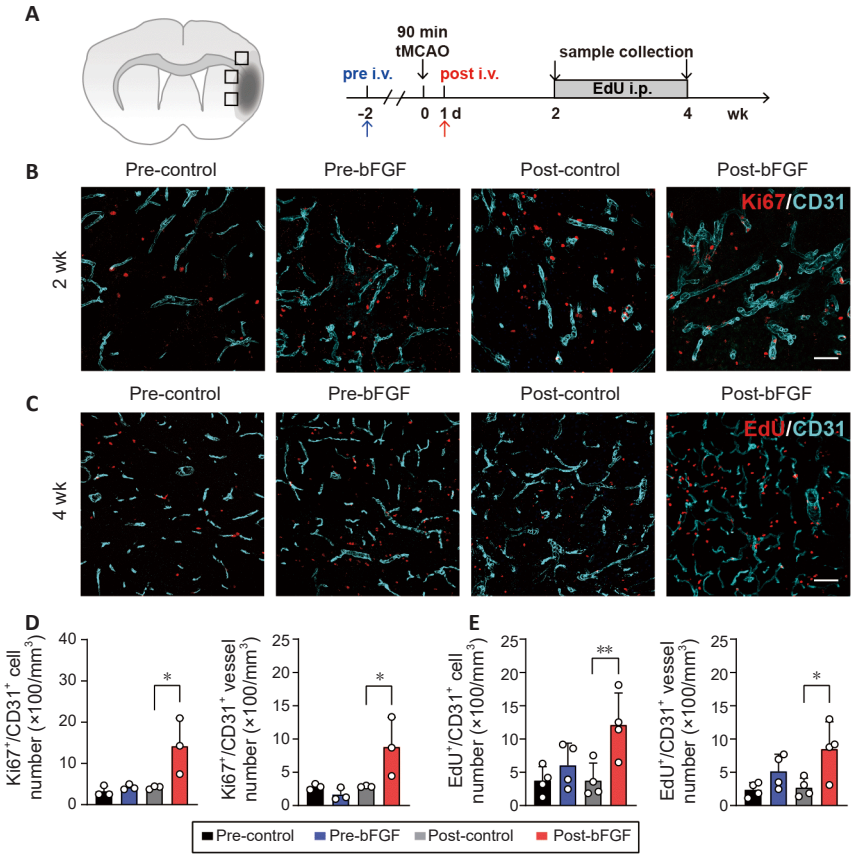

Figure 7 | AAV-PHP.eB-mediated *bFGF* gene therapy promotes angiogenesis after ischemic stroke in mice.
(A) Experimental design and diagram showing where images were taken of brain sections (boxes). Mice were injected with AAV-PHP.eB-control or AAV-PHP.eB-bFGF 14 days before tMCAO (pre-control and pre-bFGF group) or 1 day after tMCAO (post-control and post-bFGF group). (B) Representative confocal images of colocalization of Ki67 (proliferation marker, Alexa Fluor 594, red) and CD31 (endothelial cell marker, Alexa Fluor 647, cyan) in the peri-infarct area 2 weeks after tMCAO (n = 3 mice/group). Scale bar: 50 μm. The number of $Ki67^+/CD31^+$ cells increased only in the post-bFGF group compared with the control group. (C) Representative confocal images of colocalization of EdU (proliferation marker, Alexa Fluor 594, red) and CD31 (Alexa Fluor 647, cyan) in the peri-infarct area 4 weeks after tMCAO (n = 4 mice/group). Scale bar: 50 μm. The number of $EdU^+/CD31^+$ cells increased only in the post-bFGF group compared with its control group. (D, E) Statistical analysis of the number of cells and blood vessels exhibiting signal colocalization. Data are presented as mean ± SD. $^*P < 0.05$, $^{**}P < 0.01$ (ordinary one-way analysis of variance followed by Holm-Sidak correction). bFGF: Basic fibroblast growth factor; CD31: cluster of differentiation 31; EdU: 2′-deoxy-5-ethynyluridine; i.p.: intraperitoneal injection; i.v.: intravenous injection; tMCAO: transient middle cerebral artery occlusion.

(Kawamata et al., 1997; Wang et al., 2008; Ito et al., 2022). Recent efforts have focused on developing effective bFGF-based treatments for CNS injuries by developing mimetics and building novel gene delivery systems (Ardizzone et al., 2022). In our study, we used AAV-PHP.eB to carry *FGF2* gene rather than directly inject bFGF into the brain to minimize the off-target effects of bFGF as well as to provide a longer and more stable bFGF expression in the peri-infarct area. Here, we use pre-stroke administration to confirm the efficacy of bFGF in stroke therapy and post-stroke administration to investigate the feasibility of AAV-PHP.eB-bFGF as a therapeutic approach for ischemic stroke. We found that intravenous AAV-PHP.eB-mediated bFGF gene therapy successfully promoted functional recovery after ischemic stroke, with distinct effects on neurogenesis and angiogenesis when the virus was administered at different timepoints. We found that pre-stroke administration of AAV-PHP.eB-BFGF drove earlier neurogenesis, while post-stroke administration increased neurogenesis 4 weeks after tMCAO. Similarly, we observed a significant difference in angiogenesis when AAV-PHP.eB-BFGF was administered at different timepoints, with only post-stroke treatment effectively inducing angiogenesis. It is possible that these functional differences were the result of differences in cellular tropism between the two groups, since pre-stroke administration led to neuronal and astrocytic targeting, while post-stroke injection gave rise to endothelial cell tropism. We found that pre-stroke administration of AAV-PHP.eB-bFGF promoted significant behavioral recovery and alleviated brain atrophy. Although the difference in brain atrophy ratios between the post-bFGF group and the post-control group was not significant, post-stroke AAV-PHP.eB-bFGF administration did lead to long-term behavioral recovery. This might be because it provided structural and nutrient basis by generating blood vessels that eventually supported neurogenesis and possibly improved neuroplasticity and connectivity in the ipsilateral network (Grefkes and Fink, 2014; Yang et al., 2019), a possibility that should be explored in future studies. Since the pre-stroke group was injected with the virus 2 weeks earlier than the post-stroke group, it is also possible that the earlier recovery seen with pre-stroke administration was due to an earlier increase in bFGF expression. Further studies are needed to elucidate the mechanisms of action underlying this effect. To clarify the roles of different cells targeted by AAV-PHP.eB-bFGF, cell-specific promoters such as Syn (neurons), Aldh1l1 (astrocytes), and Cdh5 (endothelial cells), should be used, as well as a time course with more frequent examination.

Though AAV has long been considered safe to use in humans, its side effects still need careful investigation, since it has been reported to cause immune responses and toxicity in clinical studies (Kang et al., 2023). The immune response could cause side effects such as liver circulation damage and lead to a rapid decline in the duration of the effects of the gene therapy (Shen et al., 2022). To avoid provoking an immune response, a variety of strategies have been developed, including coadministration of immunosuppressants and the use of capsids expressing peptides that interfere with immune signaling (Bentler et al., 2023). A previous study of AAV-PHP.eB in rodent models reported a transient immune response in endothelial cells at 3 days postinjection that returned to normal levels 25 days postinjection (Brown et al., 2021).

The rapid generation of novel capsids for gene delivery has provided more options for CNS gene therapy, with noninvasive administration routes, lower levels of liver toxicity, and improved cell-specific targeting. These vectors, which have been developed in preclinical studies, could help generate gene therapies to treat CNS injuries and genetic diseases and allow researchers to revisit candidate treatments for diseases such as stroke that do not easily penetrate the BBB, such as bFGF.

There were some limitations to this study. We did not include female mice in our study, and were thus unable to explore the impact of sex on ischemic stroke recovery. In addition, the latest timepoint in our study was 28 days after tMCAO. Though we found that post-stroke AAV-PHP.eB-bFGF administration promoted endothelial cell proliferation after tMCAO, we did not demonstrate the generation of functional blood vessels. Future studies should investigate this by monitoring changes in overall cerebral perfusion using laser speckle imaging (Wang et al., 2022a) or by injecting the animals with lectin (Ritzel et al., 2017). A longer experiment and more precise promoter control are needed to investigate the effects of AAV-PHP.eB-bFGF administration on the chronic stage of ischemic stroke, its biosafety and side effects, and its effects on organs other than the brain. Furthermore, though we showed that the increased targeting to astrocytes was not due to astrocyte proliferation after tMCAO, it remains unknown where these astrocytes came from, and further studies are needed to investigate this phenomenon.

In summary, our study showed that AAV-PHP.eB cellular tropism shifted when administrated at different timepoints in a mouse model of ischemic stroke, providing a promising approach for bFGF gene therapy in ischemic stroke treatment. While the reduced neuronal tropism that we observed might not be ideal for preclinical and clinical studies of treatments targeting neurons, the preferential endothelial cell targeting that we showed could be leveraged for novel AAV-PHP.eB-based treatments.

Acknowledgments: *The syringe vector in the figures was obtained from Vecteezy.com, and the mouse vector was from pixabay.com.*
Author contributions: *YW and GYY conceived the project, designed the experiments, and revised the manuscript; RS designed and performed the experiments, analyzed the data, and drafted the manuscript and figures; JY performed the intravenous injection in tropism study and conducted flow cytometry; CW performed intravenous injection in gene therapy study and contributed to neurobehavioral assessments; ZL, SW, and QS helped with sample collection; ZL, HS, and SW helped with tMCAO modeling; YT, ZZ, XH, and WL monitored and discussed the experiment and revised the manuscript. All authors read and approved the final version of the manuscript.*
Conflicts of interest: *The authors declare no conflict of interests.*
Data availability statement: *All relevant data are within the paper and its Additional files.*

Additional files:
Additional Figure 1: *mNG$^+$ vessel diameter measurement.*
Additional Figure 2: *The tropism of AAV-PHP.eB in contralateral brain is similar to healthy brain.*

References

Aljović A, Jacobi A, Marcantoni M, Kagerer F, Loy K, Kendirli A, Bräutigam J, Fabbio L, Van Steenbergen V, Pleśniar K, Kerschensteiner M, Bareyre FM (2023) Synaptogenic gene therapy with FGF22 improves circuit plasticity and functional recovery following spinal cord injury. EMBO Mol Med 15:e16111.

Andjelkovic AV, Xiang J, Stamatovic SM, Hua Y, Xi G, Wang MM, Keep RF (2019) Endothelial targets in stroke: translating animal models to human. Arterioscler Thromb Vasc Biol 39:2240-2247.

Ardizzone A, Bova V, Casili G, Filippone A, Campolo M, Lanza M, Esposito E, Paterniti I (2022) SUN11602, a bFGF mimetic, modulated neuroinflammation, apoptosis and calcium-binding proteins in an in vivo model of MPTP-induced nigrostriatal degeneration. J Neuroinflammation 19:107.

Balkaya M, Kröber JM, Rex A, Endres M (2013) Assessing post-stroke behavior in mouse models of focal ischemia. J Cereb Blood Flow Metab 33:330-338.

Batista AR, King OD, Reardon CP, Davis C, Shankaracharya, Philip V, Gray-Edwards H, Aronin N, Lutz C, Landers J, Sena-Esteves M (2020) Ly6a differential expression in blood-brain barrier is responsible for strain specific central nervous system transduction profile of AAV-PHP.B. Hum Gene Ther 31:90-102.

Bentler M, Hardet R, Ertelt M, Rudolf D, Kaniowska D, Schneider A, Vondran FWR, Schoeder CT, Delphin M, Lucifora J, Ott M, Hacker UT, Adriouch S, Büning H (2023) Modifying immune responses to adeno-associated virus vectors by capsid engineering. Mol Ther Methods Clin Dev 30:576-592.

Bogousslavsky J, Victor SJ, Salinas EO, Pallay A, Donnan GA, Fieschi C, Kaste M, Orgogozo JM, Chamorro A, Desmet A, European-Australian Fiblast (Trafermin) in Acute Stroke Group (2002) Fiblast (trafermin) in acute stroke: results of the European-Australian phase II/III safety and efficacy trial. Cerebrovasc Dis 14:239-251.

Brown D, Altermatt M, Dobreva T, Chen S, Wang A, Thomson M, Gradinaru V (2021) Deep parallel characterization of AAV tropism and AAV-mediated transcriptional changes via single-cell RNA sequencing. Front Immunol 12:730825.

Calvani M, Rapisarda A, Uranchimeg B, Shoemaker RH, Melillo G (2006) Hypoxic induction of an HIF-1alpha-dependent bFGF autocrine loop drives angiogenesis in human endothelial cells. Blood 107:2705-2712.

Chai S, Wakefield L, Norgard M, Li B, Enicks D, Marks DL, Grompe M (2023) Strong ubiquitous micro-promoters for recombinant adeno-associated viral vectors. Mol Ther Methods Clin Dev 29:504-512.

Chan KY, Jang MJ, Yoo BB, Greenbaum A, Ravi N, Wu WL, Sánchez-Guardado L, Lois C, Mazmanian SK, Deverman BE, Gradinaru V (2017) Engineered AAVs for efficient noninvasive gene delivery to the central and peripheral nervous systems. Nat Neurosci 20:1172-1179.

Chen HH, Chien CH, Liu HM (1994) Correlation between angiogenesis and basic fibroblast growth factor expression in experimental brain infarct. Stroke 25:1651-1657.

Choudhury GR, Ding S (2016) Reactive astrocytes and therapeutic potential in focal ischemic stroke. Neurobiol Dis 85:234-244.
Duan H, Li S, Hao P, Hao F, Zhao W, Gao Y, Qiao H, Gu Y, Lv Y, Bao X, Chiu K, So KF, Yang Z, Li X (2024) Activation of endogenous neurogenesis and angiogenesis by basic fibroblast growth factor-chitosan gel in an adult rat model of ischemic stroke. Neural Regen Res 19:409-415.
Fisher M, Meadows ME, Do T, Weise J, Trubetskoy V, Charette M, Finklestein SP (1995) Delayed treatment with intravenous basic fibroblast growth factor reduces infarct size following permanent focal cerebral ischemia in rats. J Cereb Blood Flow Metab 15:953-959.
GBD 2019 Stroke Collaborators (2021) Global, regional, and national burden of stroke and its risk factors, 1990-2019: A systematic analysis for the Global Burden of Disease Study 2019. Lancet Neurol 20:795-820.
Grefkes C, Fink GR (2014) Connectivity-based approaches in stroke and recovery of function. Lancet Neurol 13:206-216.
Grødem S, Nymoen I, Vatne GH, Rogge FS, Björnsdóttir V, Lensjø KK, Fyhn M (2023) An updated suite of viral vectors for in vivo calcium imaging using intracerebral and retro-orbital injections in male mice. Nat Commun 14:608.
Guo L, Kondapavulur S, Lemke SM, Won SJ, Ganguly K (2021) Coordinated increase of reliable cortical and striatal ensemble activations during recovery after stroke. Cell Rep 36:109370.
Han Z, Luo N, Kou J, Li L, Xu Z, Wei S, Wu Y, Wang J, Ye C, Lin K, Xu F (2022) Brain-wide TVA compensation allows rabies virus to retrograde target cell-type-specific projection neurons. Mol Brain 15:13.
Hordeaux J, Yuan Y, Clark PM, Wang Q, Martino RA, Sims JJ, Bell P, Raymond A, Stanford WL, Wilson JM (2019) The GPI-linked protein LY6A Drives AAV-PHP.B transport across the blood-brain barrier. Mol Ther 27:912-921.
Huang Q, Chan KY, Tobey IG, Chan YA, Poterba T, Boutros CL, Balazs AB, Daneman R, Bloom JM, Seed C, Deverman BE (2019) Delivering genes across the blood-brain barrier: LY6A, a novel cellular receptor for AAV-PHP.B capsids. PLoS One 14:e0225206.
Ito Y, Oyane A, Yasunaga M, Hirata K, Hirose M, Tsurushima H, Ito Y, Matsumaru Y, Ishikawa E (2022) Induction of angiogenesis and neural progenitor cells by basic fibroblast growth factor-releasing polyglycolic acid sheet following focal cerebral infarction in mice. J Biomed Mater Res A 110:1964-1975.
Jang S, Shen HK, Ding X, Miles TF, Gradinaru V (2022) Structural basis of receptor usage by the engineered capsid AAV-PHP.eB. Mol Ther Methods Clin Dev 26:343-354.
Jiang L, Li W, Mamtilahun M, Song Y, Ma Y, Qu M, Lu Y, He X, Zheng J, Fu Z, Zhang Z, Yang GY, Wang Y (2017) Optogenetic inhibition of striatal GABAergic neuronal activity improves outcomes after ischemic brain injury. Stroke 48:3375-3383.
Kang L, Jin S, Wang J, Lv Z, Xin C, Tan C, Zhao M, Wang L, Liu J (2023) AAV vectors applied to the treatment of CNS disorders: Clinical status and challenges. J Control Release 355:458-473.
Kawamata T, Dietrich WD, Schallert T, Gotts JE, Cocke RR, Benowitz LI, Finklestein SP (1997) Intracisternal basic fibroblast growth factor enhances functional recovery and up-regulates the expression of a molecular marker of neuronal sprouting following focal cerebral infarction. Proc Natl Acad Sci U S A 94:8179-8184.
Kucharz K, Kristensen K, Johnsen KB, Lund MA, Lønstrup M, Moos T, Andresen TL, Lauritzen MJ (2021) Post-capillary venules are the key locus for transcytosis-mediated brain delivery of therapeutic nanoparticles. Nat Commun 12:4121.
Lazarous DF, Shou M, Stiber JA, Dadhania DM, Thirumurti V, Hodge E, Unger EF (1997) Pharmacodynamics of basic fibroblast growth factor: Route of administration determines myocardial and systemic distribution. Cardiovasc Res 36:78-85.
Lemmerman LR, Harris HN, Balch MHH, Rincon-Benavides MA, Higuita-Castro N, Arnold DW, Gallego-Perez D (2022) Transient middle cerebral artery occlusion with an intraluminal suture enables reproducible induction of ischemic stroke in mice. Bio Protoc 12:e4305.
Li M, Xu TM, Zhang DY, Zhang XM, Rao F, Zhan SZ, Ma M, Xiong C, Chen XF, Wang YH (2023) Nerve growth factor-basic fibroblast growth factor poly-lactide co-glycolid sustained-release microspheres and the small gap sleeve bridging technique to repair peripheral nerve injury. Neural Regen Res 18:162-169.
Lin TN, Te J, Lee M, Sun GY, Hsu CY (1997) Induction of basic fibroblast growth factor (bFGF) expression following focal cerebral ischemia. Brain Res Mol Brain Res 49:255-265.
Liu D, Zhu M, Lin Y, Li M, Huang R, Yang L, Song Y, Diao Y, Yang C (2022) LY6E protein facilitates adeno-associated virus crossing in a biomimetic chip model of the human blood-brain barrier. Lab Chip 22:4180-4190.
Mathiesen SN, Lock JL, Schoderboeck L, Abraham WC, Hughes SM (2020) CNS transduction benefits of AAV-PHP.eB over AAV9 are dependent on administration route and mouse strain. Mol Ther Methods Clin Dev 19:447-458.
Matsumoto K, Mitani TT, Horiguchi SA, Kaneshiro J, Murakami TC, Mano T, Fujishima H, Konno A, Watanabe TM, Hirai H, Ueda HR (2019) Advanced CUBIC tissue clearing for whole-organ cell profiling. Nat Protoc 14:3506-3537.
Nian K, Harding IC, Herman IM, Ebong EE (2020) Blood-brain barrier damage in ischemic stroke and its regulation by endothelial mechanotransduction. Front Physiol 11:605398.
Paxinos G, Franklin KB (2001) The mouse brain in stereotaxic coordinates. New York: Academic Press.
Percie du Sert N, et al. (2020) The ARRIVE guidelines 2.0: updated guidelines for reporting animal research. PLoS Biol 18:e3000410.
Ritzel RM, Patel AR, Spychala M, Verma R, Crapser J, Koellhoffer EC, Schrecengost A, Jellison ER, Zhu L, Venna VR, McCullough LD (2017) Multiparity improves outcomes after cerebral ischemia in female mice despite features of increased metabovascular risk. Proc Natl Acad Sci U S A 114:E5673-E5682.
Salic A, Mitchison TJ (2008) A chemical method for fast and sensitive detection of DNA synthesis in vivo. Proc Natl Acad Sci U S A 105:2415-2420.
Schaar KL, Brenneman MM, Savitz SI (2010) Functional assessments in the rodent stroke model. Exp Transl Stroke Med 2:13.
Schindelin J, Arganda-Carreras I, Frise E, Kaynig V, Longair M, Pietzsch T, Preibisch S, Rueden C, Saalfeld S, Schmid B, Tinevez JY, White DJ, Hartenstein V, Eliceiri K, Tomancak P, Cardona A (2012) Fiji: an open-source platform for biological-image analysis. Nat Methods 9:676-682.
Shen W, Liu S, Ou L (2022) rAAV immunogenicity, toxicity, and durability in 255 clinical trials: A meta-analysis. Front Immunol 13:1001263.
Sheng WS, Xu HL, Zheng L, Zhuang YD, Jiao LZ, Zhou JF, ZhuGe DL, Chi TT, Zhao YZ, Lan L (2018) Intrarenal delivery of bFGF-loaded liposome under guiding of ultrasound-targeted microbubble destruction prevent diabetic nephropathy through inhibition of inflammation. Artif Cells Nanomed Biotechnol 46:373-385.
Shi X, Luo L, Wang J, Shen H, Li Y, Mamtilahun M, Liu C, Shi R, Lee JH, Tian H, Zhang Z, Wang Y, Chung WS, Tang Y, Yang GY (2021) Stroke subtype-dependent synapse elimination by reactive gliosis in mice. Nat Commun 12:6943.
Sun D, Wang W, Wang X, Wang Y, Xu X, Ping F, Du Y, Jiang W, Cui D (2018) bFGF plays a neuroprotective role by suppressing excessive autophagy and apoptosis after transient global cerebral ischemia in rats. Cell Death Dis 9:172.
Sun F, Jiang F, Zhang N, Li H, Tian W, Liu W (2020) Upregulation of Prickle2 ameliorates Alzheimer's disease-like pathology in a transgenic mouse model of Alzheimer's disease. Front Cell Dev Biol 8:565020.
Suo Q, Deng L, Chen T, Wu S, Qi L, Liu Z, He T, Tian HL, Li W, Tang Y, Yang GY, Zhang Z (2023) Optogenetic activation of astrocytes reduces blood-brain barrier disruption via IL-10 In stroke. Aging Dis 14:1870-1886.
Toth AE, Siupka P, TJ PA, Venø ST, Thomsen LB, Moos T, Lohi HT, Madsen P, Lykke-Hartmann K, Nielsen MS (2018) The endo-lysosomal system of brain endothelial cells is influenced by astrocytes in vitro. Mol Neurobiol 55:8522-8537.
Wang C, Yang X, Jiang Y, Qi L, Zhuge D, Xu T, Guo Y, Deng M, Zhang W, Tian D, Yin Q, Li L, Zhang Z, Wang Y, Yang GY, Chen Y, Tang Y (2022a) Targeted delivery of fat extract by platelet membrane-cloaked nanocarriers for the treatment of ischemic stroke. J Nanobiotechnology 20:249.
Wang LL, Serrano C, Zhong X, Ma S, Zou Y, Zhang CL (2021) Revisiting astrocyte to neuron conversion with lineage tracing in vivo. Cell 184:5465-5481.e16.
Wang Y, Wang D, Wu C, Wang B, He S, Wang H, Liang G, Zhang Y (2022b) MMP 9-instructed assembly of bFGF nanofibers in ischemic myocardium to promote heart repair. Theranostics 12:7237-7249.
Wang ZL, Cheng SM, Ma MM, Ma YP, Yang JP, Xu GL, Liu XF (2008) Intranasally delivered bFGF enhances neurogenesis in adult rats following cerebral ischemia. Neurosci Lett 446:30-35.
Williamson MR, Jones TA, Drew MR (2019) Functions of subventricular zone neural precursor cells in stroke recovery. Behav Brain Res 376:112209.
Wu Y, Sun J, Lin Q, Wang D, Hai J (2024) Sustained release of vascular endothelial growth factor A and basic fibroblast growth factor from nanofiber membranes reduces oxygen/glucose deprivation-induced injury to neurovascular units. Neural Regen Res 19:887-894.
Xiao D, Zhang W, Wang Q, Li X, Zhang Y, Rasouli J, Casella G, Ciric B, Curtis M, Rostami A, Zhang GX (2021) CRISPR-mediated rapid generation of neural cell-specific knockout mice facilitates research in neurophysiology and pathology. Mol Ther Methods Clin Dev 20:755-764.
Xie BS, Wang X, Pan YH, Jiang G, Feng JF, Lin Y (2021) Apolipoprotein E, low-density lipoprotein receptor, and immune cells control blood-brain barrier penetration by AAV-PHP.eB in mice. Theranostics 11:1177-1191.
Yang Y, Chen Y, Chen K, Wei D, Li P, Zeng W, Pei J, Mao H, Jia J, Zhang Z (2019) Increased intrinsic connectivity for structural atrophy and functional maintenance after acute ischaemic stroke. Eur J Neurol 26:935-942.
Yuan M, Tang Y, Huang T, Ke L, Huang E (2024) In situ direct reprogramming of astrocytes to neurons via polypyrimidine tract-binding protein 1 knockdown in a mouse model of ischemic stroke. Neural Regen Res 19:2240-2248.
Zheng Z, Li G, Cui C, Wang F, Wang X, Xu Z, Guo H, Chen Y, Tang H, Wang D, Huang M, Chen ZY, Huang X, Li H, Li GL, Hu X, Shu Y (2022) Preventing autosomal-dominant hearing loss in Bth mice with CRISPR/CasRx-based RNA editing. Signal Transduct Target Ther 7:79.
Zhou R, et al. (2022) A signalling pathway for transcriptional regulation of sleep amount in mice. Nature 612:519-527.

C-Editor: Zhao M; S-Editors: Yu J, Li CH; L-Editors: Crow E, Yu J, Song LP; T-Editor: Jia Y

趋向性转变的 AAV-PHP.eB 介导的 bFGF 基因治疗促进小鼠缺血性脑卒中后的多样化神经修复
文章特色分析

一、文章重要性

1. 为脑卒中基因治疗提供了新策略

本研究聚焦于 AAV-PHP.eB 这一能高效穿越血脑屏障的腺相关病毒载体，结合 bFGF（碱性成纤维细胞生长因子） 基因，系统性地探讨了其在缺血性脑卒中模型中的治疗潜力。bFGF 虽在临床前期研究中表现出促进神经修复的作用，但因半衰期短、系统性给药副作用大等问题，临床转化受限。本研究通过基因治疗手段实现 bFGF 的长期、稳定表达，为脑卒中治疗提供了新的思路。

2. 揭示了 AAV 载体在病理状态下的趋向性变化

研究发现，AAV-PHP.eB 在脑卒中后的细胞趋向性发生显著转变：从健康状态下的神经元为主，转变为卒中后的内皮细胞和星形胶质细胞。这一发现提示，病毒载体的使用时机和病理背景对其靶向性具有决定性影响，对基因治疗的精准设计具有重要指导意义。

二、创新性特色

1. 首次系统揭示 AAV-PHP.eB 在脑卒中模型中的趋向性变化

- 在健康小鼠中，AAV-PHP.eB 主要感染神经元；
- 在卒中后给药（尤其是卒中后第 1 天），其趋向性显著转向内皮细胞，并与 Ly6A 受体表达上调密切相关；
- 这一趋向性转变具有时间依赖性，仅在卒中早期（Ly6A 高表达期）出现。

2. 基于趋向性转变设计差异化治疗策略

- 卒中前给药：主要靶向神经元和星形胶质细胞，促进早期神经发生；
- 卒中后给药：主要靶向内皮细胞，促进血管生成；
- 两种策略均能改善神经功能恢复，但作用机制和时序不同。

3. 实现 bFGF 的长期、局部、稳定表达

通过 AAV 介导的基因递送，克服了重组 bFGF 蛋白半衰期短、系统性副作用大的问题，为 bFGF 的临床应用提供了新路径。

三、对学科的启示

1. 强调病毒载体趋向性在疾病状态下的动态变化

本研究提示，病毒载体的趋向性并非固定不变，而是受疾病状态、给药时机、受体表达等多种因素影响。未来在设计基因治疗策略时，必须考虑病理微环境对载体行为的影响。

2. 为“时序精准治疗”提供依据

研究显示，不同给药时机导致不同的细胞靶向与修复机制：早期神经发生 vs. 晚期血管生成。这提示在脑卒中治疗中，可根据疾病阶段选择最佳干预时机与靶点，实现“时序个性化治疗”。

3. 推动非侵入性基因治疗的发展

AAV-PHP.eB 可通过静脉注射实现中枢神经系统的高效转染，避免了颅内注射的创伤性，具有更高的临床转化潜力。

4. 为其他神经退行性或血管性疾病的基因治疗提供借鉴

该研究不仅适用于脑卒中，其发现的趋向性机制和治疗策略也可推广至其他中枢神经系统疾病，如阿尔茨海默病、脑外伤等。

总结

本研究通过揭示 AAV-PHP.eB 在脑卒中模型中的趋向性转变，并基于此设计出具有时序差异的 bFGF 基因治疗策略，不仅在机制研究上有重要突破，也为脑卒中的基因治疗提供了新的理论与实践基础。其创新性在于将病毒趋向性动态变化与治疗时序策略相结合，推动了基因治疗向更精准、更个性化的方向发展。